Journal of Power Sources 224 (2013) 139–144

Contents lists available at SciVerse ScienceDirect

Journal of Power Sources

journal homepage: www.elsevier.com/locate/jpowsour

A new method for fabrication of graphene/polyaniline nanocomplex modified microbial fuel cell anodes

Junxian Hou, Zhongliang Liu*, Peiyuan Zhang

Key Laboratory of Enhanced Heat Transfer and Energy Conservation, Ministry of Education and Key Laboratory of Heat transfer and Energy Conversion, Beijing Education Commission, College of Environmental and Energy Engineering, Beijing University of Technology, Beijing 100124, PR China

HIGHLIGHTS

- We provide a new and effective electrode modification method for microbial fuel cell electrodes.
- Graphene is prepared using an electrochemical synthesis method reducing graphene oxide by cyclic voltammetry.
- PANI–ERGNO/CC greatly improves the bacterial biofilm loading and the charge transfer efficiency.

ARTICLE INFO

Article history:
Received 2 August 2012
Received in revised form
25 September 2012
Accepted 27 September 2012
Available online 4 October 2012

Keywords:
Microbial fuel cell
Electrode modification
Electrochemically reducing graphene oxide
Graphene nano-sheets
Polyaniline nano-fibers

ABSTRACT

A novel microbial fuel cell (MFC) anode is fabricated by electrochemically reducing graphene oxide (ERGNO) first and coating polyaniline (PANI) nano-fibers afterward on the surface of carbon cloth (CC). ERGNO/CC is prepared using an electrochemical synthesis method reducing graphene oxide by cyclic voltammetry (CV) in phosphate buffer solution (PBS, pH = 6.9). Combining the advantages of PANI and ERGNO, PANI–ERGNO/CC yields a maximum power density of 1390 mW m^{-2} when used as the MFC anode, which is 3 times larger than that of the MFC with the CC anode. The electrodes are characterized by scanning electron microscopy (SEM) and Raman spectroscopy. The electrochemical activities have been investigated by CV and electrochemical impedance spectroscopy (EIS). The great improvement is attributed to the fact that graphene not only serves as a highly conductive support material, but also provides large surface for PANI. High conductivity and large specific surface area greatly improve the charge transfer efficiency and the bacterial biofilm loading. In this work, a practical and promising synthesis method is developed to fabricate high-performance MFC anodes.

1. Introduction

Microbial fuel cells (MFCs) convert chemical energy into electrical energy directly via electro-active micro-organisms, and have a great potential application for simultaneous wastewater treatment and energy recovery which is its main advantage over other conventional wastewater treatment methods [1]. MFC-based technologies such as microbial electrolysis cell [2,3], microbial desalination cell [4,5] and biosensor [6] have great promising applications. However, the low power density of MFCs remains one of the main obstacles for their practical applications. The total energy loss in the MFC system can be understood from the voltage equation, $V = E_t - \eta_{act} - \eta_{ohmic} - \eta_{conc.}$, in which η_{act}, η_{ohmic} and η_{conc} are voltage losses due to reaction kinetics, ohmic polarization and mass transport, respectively. Reaction kinetics directly affects electrode reaction rate. So, the basic way to optimize the anode that serves as both a carrier of bacteria and an electron collector in MFCs is to facilitate the electrons transfer and thus to improve the MFC overall performance [7]. The anode surface characteristics, such as surface area, surface potential, surface biocompatibility, and surface roughness significantly affect the anodic reaction. Various nano-structured materials such as carbon nanotube [8,9], PANI [10] and ruthenium oxide [11] had been used to modify the MFC electrodes to minimize the anode energy loss in the system and have significantly increased the MFC power density output.

Graphene is a single-atom-thick sheet consisting of sp^2 hybridized carbon atoms which is the building block of all graphitic carbons. Graphene has attracted tremendous interests due to its unique properties including high electronic conductivity, high modulus, and high specific surface area ($\sim 2.6 \times 10^3$ m^2 g^{-1}) [12]. These unique properties have led to numerous efforts applying graphene in both electronic devices and composite materials, such

* Corresponding author. Tel./fax: +86 (0)10 67391917.
E-mail address: liuzhl@bjut.edu.cn (Z. Liu).

0378-7753/$ – see front matter © 2012 Elsevier B.V. All rights reserved.
http://dx.doi.org/10.1016/j.jpowsour.2012.09.091

as supercapacitors [13], solar cells [14] and lithium ion batteries [15]. Zhang et al. perhaps are the first to use graphene for MFC. They used graphene (264 $m^2 g^{-1}$) modified stainless steel mesh (GMS) as MFC anode and obtained a power density of 2668 mW m^{-2} which is 18 times larger than the unmodified one [16]. The largest maximum power density by use of the crumpled graphene-modified anode electrode in MFC is 3.6 W m^{-3}, twice of that of the activated carbon-modified anode electrode (1.7 W m^{-3}) [17]. In reference, graphene was electrochemically deposited on carbon cloth to fabricate an anode, and the graphene modification improved power density and energy conversion efficiency by 2.7 and 3 times, respectively [18]. Recently, a macroporous and monolithic MFC anode based on polyaniline hybridized three-dimensional (3D) graphene has been demonstrated that the maximum power density obtained from the 3D graphene/PANI MFC (~768 mW m^{-2}) is about 4 times higher than that from the carbon cloth MFC (~158 mW m^{-2}). The fact that the graphene associated with polyaniline modification MFC electrode outperforms the planar carbon electrode is due to its abilities to form three-dimensional interface with bacterial biofilm, facilitate electron transfer, and provide multiplexed and highly conductive pathways [19]. Furthermore, the graphene-based polymer nanocomposites have much better electrical properties than other carbon filler-based polymer nano-composites [20]. Graphene modified electrodes are usually fabricated by the following methods. The first method involves direct deposition of graphene onto a conductive substrate by drop casting graphene solution obtained from chemical reduction of graphene oxide (GNO) sheets [16,17]. The second involves electrochemical reduction of graphene oxide to graphene, either from a graphene oxide film on the electrode surface or from a solution containing dissolved graphene oxide. In this way, the thickness of the resulting films was uniform, controllable and reproducible, and moreover, toxic chemicals were not involved [21].

In the present study, ERGNO/CC was prepared using an electrochemical synthesis method reducing GNO by scanning the potential between 0 and −1.6 V vs a Ag/AgCl electrode in phosphate buffer solution (PBS, pH = 6.9), and was applied to MFC anode for the first time. Using PANI–ERGNO/CC and ERGNO/CC as the MFC anodes, the maximum power density obtained is 1390 mW m^{-2} and 1003 mW m^{-2}, respectively, which is 3 and 2.1 times larger than the MFC with CC anode. The excellent performance is not only because that the graphene can provide good electrical conductivity and high specific surface area, but also due to the fact that PANI nano-fibers possess good redox activity and biocompatibility.

2. The experimental

2.1. Chemicals and materials

Graphite oxide (GO) was produced by Nanjing XF Nano Materials S&T Co. Ltd., and was synthesized by the Hummers method [22]. Carbon cloth was supplied by Shanghai Hesen Electric Co. Ltd. Carbon felt was produced by Beiing Sanye Co. Ltd. All chemicals were of analytical reagent grade and used without further purification. De-ionized water was used in the experiments.

Graphene oxide (GNO) was obtained by the ultrasound treatment of 1 mg mL^{-1} graphite oxide dispersion in a Sonifier (KQ500DA, Kunshan, China) for 3 h at 400 W. Only the upper solution was collected and used after leaving the obtained brown dispersion aside for settling one week to avoid any un-exfoliated graphite oxide [23]. PANI solution was synthesized by a rapid mixing reaction. The purified aniline (0.3 g, 3.2 mmol) was dissolved in 10 mL of 1 M HCl aqueous solution. While maintaining vigorous stirring at room temperature, ammonium peroxydisulfate (0.18 g, 0.8 mmol) in 10 mL of 1 M HCl aqueous solution was poured into the aniline solution rapidly. Polymerization was observed in about 5 min when the characteristic green color of polyaniline emeraldine salt appeared. The mixture was stirred at room temperature overnight before use [24].

2.2. Electrode fabrication

Carbon cloth (1.8 cm × 1.8 cm) was soaked in acetone for 5 h and then rinsed with the ultrapure water until its pH value equals to 7, and finally dried under vacuum at 60 °C. The ERGNO/CC was obtained using the method suggested by Du et al. [25]. The GNO/CC was prepared by dripping 1 mg mL^{-1} GNO suspension onto the CC surface using layer by layer method, and after rinsed with the ultrapure water it was dried naturally in the air. The final loading of the GNO was about 2 mg. The electrochemical reduction of GNO/CC was carried out with cyclic voltammetry (0 V to −1.6 V, 5 mV s^{-1}) in 100 mM PBS (10.7 g L^{-1} K_2HPO_4, 5.3 g L^{-1} KH_2PO_4, pH = 6.9) in a standard three-electrode cell with the Ag/AgCl and Pt mesh as the reference and counter electrode, respectively (all electrode potentials are scaled to reversible hydrogen electrode (RHE) unless otherwise specified). PANI–ERGNO/CC was prepared by immersing ERGNO/CC in the PANI solution obtained above for 12 h, then rinsed with the ultrapure water until it is neutral (pH = 7) and dried naturally in the air.

2.3. MFC construction and operation

MFCs consisting of two cylindrical compartments of equal dimensions (2 cm deep, 20 cm^2 of the cross sectional area) were built. The two compartments were separated by Nafion 117 (DuPont, USA) and the volume of each compartment was 40 mL. The anode chambers were inoculated with the anaerobic sludge from Beijing Gaobeidian Wastewater Treatment Plant. Anolyte consisted of 1 g L^{-1} CH_3COONa, 0.3 g L^{-1} NH_4Cl, 1 g L^{-1} NaCl, 0.04 g L^{-1} $CaCl_2 \cdot 2H_2O$, 0.3 g L^{-1} $MgSO_4$, 0.2 g L^{-1} $NaHCO_3$, 10.7 g L^{-1} K_2HPO_4, 5.3 g L^{-1} KH_2PO_4, and 1 mL trace elements [26]. Carbon felts (2 cm × 2 cm) were chosen as the cathode of the MFCs. The cathodic compartment of all MFCs was filled with 50 mM ferricyanide and 100 mM phosphate buffer solution (10.7 g L^{-1} K_2HPO_4, 5.3 g L^{-1} KH_2PO_4, pH = 6.9). The MFCs were operated under the fed-batch mode condition, and the anolyte was replaced after the voltage below 50 mV. All experiments were carried out at the constant temperature (30 ± 0.5 °C) with a 500 Ω external resistance connected unless otherwise specified.

2.4. Measurement and analysis

The cell voltage was recorded every 5 min by a digital multimeter (UT70D, Uni-Trend Group Ltd). The cyclic voltammograms (CVs) were performed using the CHI660D (Shanghai, CH Instruments) at a scan rate of 5 mV s^{-1} in a three-electrode cell. The anode electrode, the Pt electrode and the Ag/AgCl were used as the working electrode, the counter electrode and the reference electrode, respectively. EIS measurements were also conducted in a three electrode mode by recording the impedance spectrum of the anodes between 100 kHz and 5 mHz at open-circuit potential with a perturbation signal of 10 mV. Polarization curves were obtained by varying the external resistor over a range from 50 Ω to 9999 Ω to monitor the MFC steady state current. The surface chemistry of the functionalized GNO, ERGNO, PANI and PANI–ERGNO on the carbon cloth was analyzed using Raman spectroscopy (JY-T64000). SEM (Hitachi S-4300N) was employed to characterize the surface microstructure of the anodes.

3. Results and discussion

3.1. Reduction process of GNO/CC

Fig. 1 shows the cyclic voltammograms of the GNO-modified carbon cloth (GNO/CC) in a potential range between 0 and −1.6 V in PBS (pH = 6.9) saturated with nitrogen gas (N_2). From this figure, one can see that the GNO/CC shows a much larger peak cathodic current at −1.5 V (vs. Ag/AgCl) with a starting potential of −0.6 V (vs. Ag/AgCl) in the first cycle than that of the CC. This reduction peak could be due to the reduction of the surface oxygen groups, such as −OH, −COOH, and epoxides at GNO, indicating that the GNO could indeed be reduced electrochemically to form ERGNO/CC, agreeing well with the previous reports [23,27,28]. In the second cycle, the reduction current at negative potentials decreases considerably and disappears after several potential scans. This demonstrates that the reduction of surface-oxygenated species at GNO occurs quickly and irreversibly and the GNO have been reduced electrochemically at negative potentials. ERGNO film has been obtained on carbon cloth [23,29].

3.2. Microstructure characterization of the anodes

Raman spectroscopy is a powerful non-destructive tool to distinguish ordered and disordered crystal structures of carbon. Fig. 2 shows the Raman spectra of the CC, GNO/CC, ERGNO/CC, PANI/CC, PANI–ERGNO/CC samples. The Raman spectrum of CC (Fig. 2e) shows two peaks at 1344 cm^{-1} and 1589 cm^{-1} corresponding to the D and G bands of the CC due to disordered and graphitic phases, respectively, and this indicated a microcrystalline graphite structure. The D band at 1348 cm^{-1} and G band at 1585 cm^{-1} are observed in the Raman spectrum of the GNO/CC (Fig. 2d), ERGNO/CC (Fig. 2c), and PANI–ERGNO/CC (Fig. 2a) samples. The D band represents breathing modes of rings or K-point phonons of A_{1g} symmetry, while the G band corresponds to the in-plane bond-stretching motion of the pairs of C sp^2 atoms [30]. When the exfoliated GO is electrochemically reduced, the intensity of the D band increases further. This may be due to the defects introduced into the ERGNO during the preparation process [31,32]. In addition, the weak and broadened 2D peak shows that ERGNO possesses some defects because of the fast reduction rate. These local defects can hardly recover in time. These defects could be further eliminated by performing the electrochemical reduction

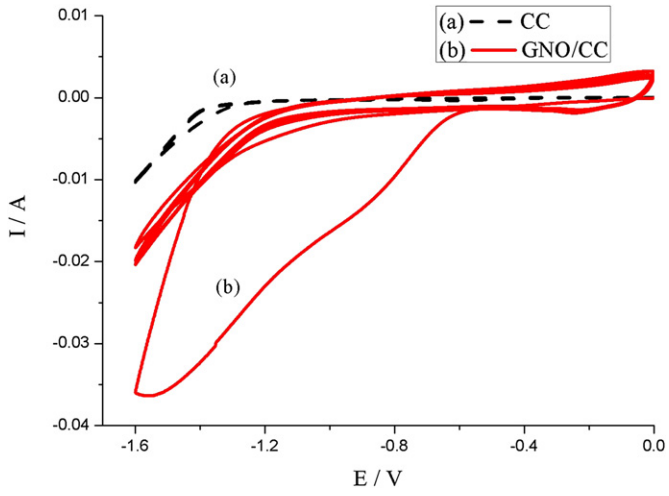

Fig. 1. Cyclic voltammograms of CC (a) and GNO/CC (b) in PBS (pH = 6.9) saturated with N_2 at a scan rate of 5 mV s^{-1}.

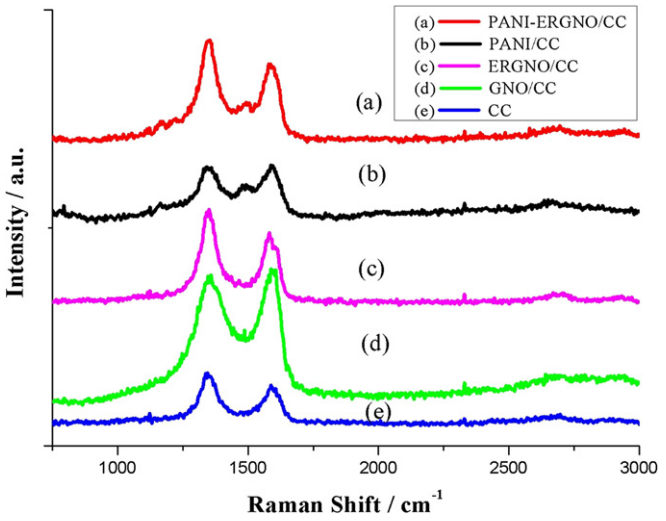

Fig. 2. Raman spectrum of PANI–ERGNO/CC (a), PANI/CC (b), ERGNO/CC (c), GNO/CC (d), and CC (e).

at an elevated temperature or annealing the products [23]. However, an increased D/G intensity ratio of ERGNO compared to that of GNO is observed. This change suggests a decrease in the average size of the sp^2 domains due to reduction of GNO and can be explained by the creation of numerous new graphitic domains that are smaller in size than the ones presented in GNO [23]. The spectrum of the pure PANI (Fig. 2b) exhibits some typical bands of the C–H bending of the quinoid ring at 1162 cm^{-1}, C–N^+ stretching of the bipolar on structure at 1338 cm^{-1}, C=N stretching vibration at 1468 cm^{-1} and C=C stretching of the benzenoid ring at 1590 cm^{-1}. The new peaks arising from PANI at 1167 cm^{-1} and 1468 cm^{-1} also appear in the Raman spectrum of PANI–ERGNO/CC, which correspond to C–H bending of the quinoid ring and N–H bending of bipolaronic structure, respectively [33,34]. The presence of these new peaks indicates the presence of the PANI on the surfaces of the ERGNO.

The morphologies of the GNO/CC, the ERGNO/CC and the PANI–ERGNO/CC were examined by scanning electron microscopy (SEM). Compared with Fig. 3(a), the thin wrinkled and crumpled structures as shown Fig. 3(b) are typical of ERGNO sheets after electrochemical reduction from GNO, agreeing well with the previous results [28,35,36]. Fig. 3(c) shows the SEM image of PANI–ERGNO/CC after PANI was deposited on the graphene film. Obviously, it further proves that the present method is effective for forming PANI–ERGNO hybrid coating on CC in this study.

3.3. Electrochemical analysis

CV tests were carried out to determine the electrocatalytic behavior of the anode materials. As revealed in Fig. 4, the voltammograms of the PANI–ERGNO/CC, the ERGNO/CC and PANI/CC showed larger currents than that of the CC anode electrode, indicating that these anodes have either an enhanced surface area or an optimized structure [16,17]. As shown in Fig. 4, the ERGNO/CC CV displayed the redox peaks at −0.47 V and −0.12 V. Two couples of the redox peaks were observed from the CV curve of the PANI/CC attributed to the redox of PANI, corresponding to its leucoemeraldine/emeraldine and emeraldine/pernigraniline structural conversions, respectively [37]. Similarly, PANI–ERGNO/CC also exhibited two couples of the redox peaks which were larger than ERGNO/CC and PANI/CC as a result of the advantages of PANI and ERGNO. A peak current of 0.6 mA at −0.05 V in the oxidation scan and a peak current of −1.28 mA at −0.5 V in the reduction scan

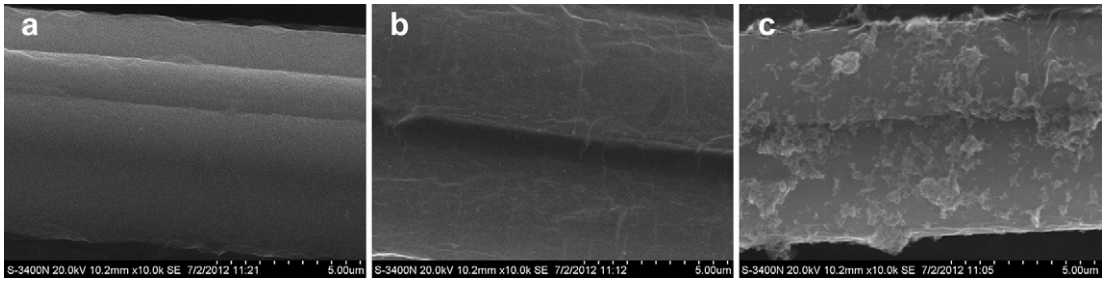

Fig. 3. SEM images of GNO/CC (a), ERGNO/CC (b), and PANI–ERGNO/CC (c).

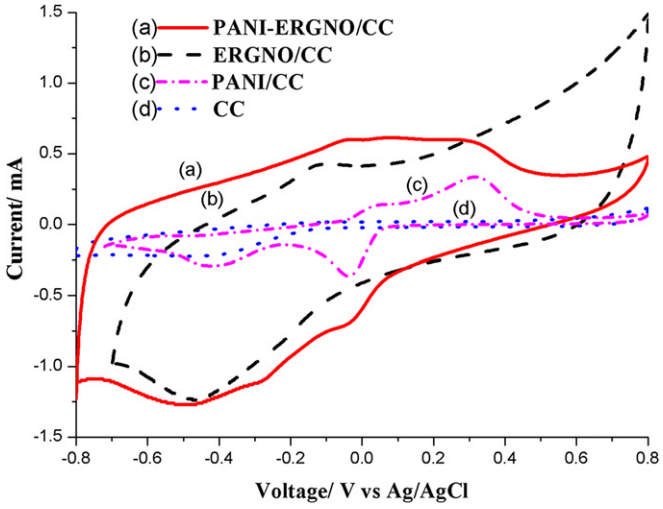

Fig. 4. CVs of PANI–ERGNO/CC (a), ERGNO/CC (b), PANI/CC (c) and CC (d) in 100 mM PBS (−0.8 V to 0.8 V, 5 mV s^{-1}).

were observed at the PANI–ERGNO/CC obviously. The peak current of the PANI–ERGNO/CC was much larger than that of ERGNO/CC and PANI/CC. This may be contributed to the enhanced electron-transfer efficiency resulted from the inherent properties of graphene and PANI.

Electrochemical impedance spectroscopy (EIS) analysis was then carried out to investigate the charge-transfer resistance of the different anodes (Fig. 5). The EIS Nyquist plot is the superimposition of a preceding frequency-dependent semi-circle (high frequency region) and a subsequent straight line (low frequency region), the diameter of the former represents the charge-transfer resistance [38]. The equivalent circuit used here assumes that the anode reaction is affected by both reaction kinetics and diffusion (Fig. 1), with the symbol R_s for solution resistance and R_{ct} for charge transfer resistance. A constant phase element (CPE) is used instead of a capacitor in order to model double layer capacitance when surface roughness or a distribution of reactions across the surface possibly affect overall kinetics [10,39]. By fitting the data of the Nyquist plots using the Zview program, we obtained the values of each parameter. The solution resistances (R_s), resulting from the ionic resistance of electrolyte, the intrinsic resistance of active materials, and the contact resistance, were all about 10 Ω for different electrodes. The charge-transfer resistance (R_{ct}) which represents the resistance of electrochemical reactions on the electrode, behaved differently. The unmodified carbon cloth had a polarization resistance of 47 Ω is much larger than that of PANI–ERGNO/CC (~16 Ω), ERGNO (~9 Ω) and PANI/CC (~18 Ω). A smaller charge-transfer resistance is resulted from a faster electron transfer rate. This confirms that the electron transfer efficiency of the PANI–ERGNO/CC is much higher than that of the CC. Additionally, The straight line region over low frequency of ERGNO/CC and PANI–

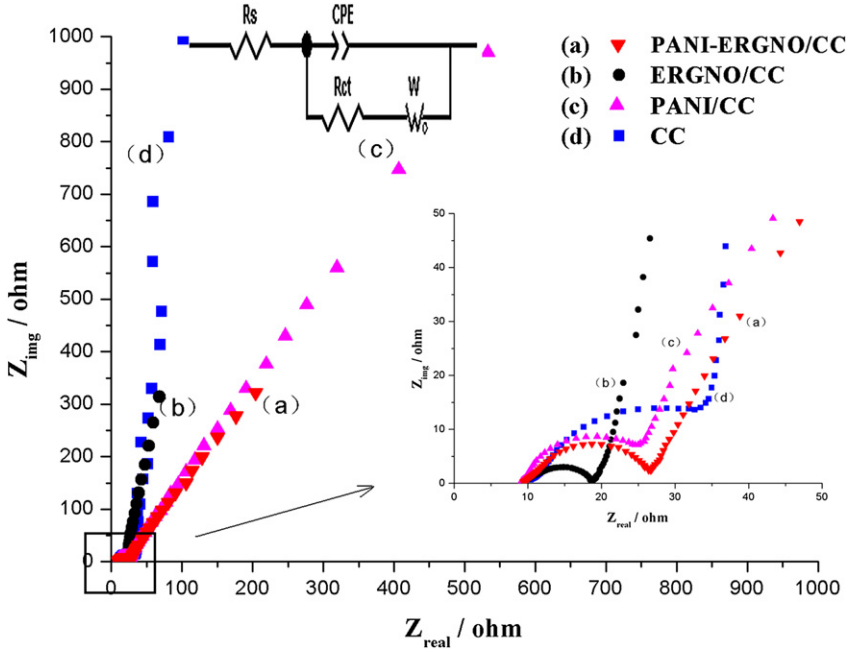

Fig. 5. EIS of PANI–ERGNO/CC (a), ERGNO/CC (b), PANI/CC (c) and CC (d) in 100 mM PBS at open-circuit potential (5 mHz ~ 100 kHz).

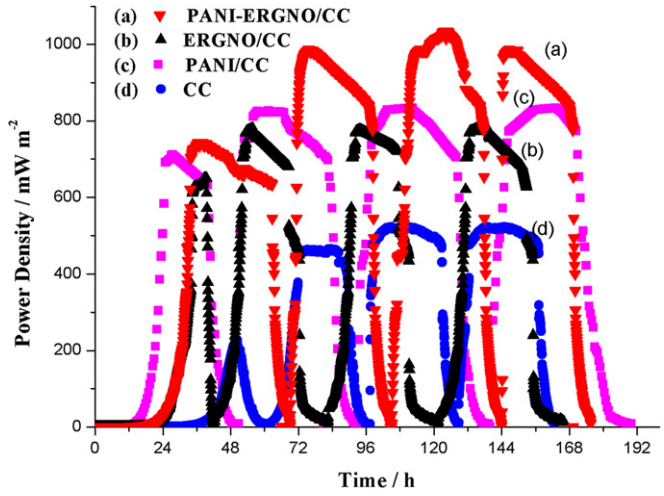

Fig. 6. Power density output of the MFCs with PANI–ERGNO/CC (a), ERGNO/CC (b), PANI/CC (c) and CC (d).

ERGNO/CC electrodes was significantly smaller than that of PANI/CC and CC electrode. The straight line region is usually characteristic of a diffusion-limiting step in an electrochemical process. This indicates that PANI–ERGNO/CC and ERGNO/CC have a good micro/nanostructure for reactants to access the reaction centers [10], and obviously improve the diffusion of electrolyte toward the electrode surface. Both CV and EIS results have demonstrated that the PANI–ERGNO/CC electrode exhibited a favorable and stable electrochemical behavior.

3.4. Power curve

The large specific surface area for bacterial adhesion and high charge transfer efficiency of the PANI–ERGNO/CC, the PANI/CC and ERGNO/CC anodes would greatly improve their power density output over the CC anode. To verify this, the performance of the four types of the anodes was operated simultaneously with an external resistance of 500 Ω. As shown in Fig. 6, the power density of the MFCs with the PANI–ERGNO/CC, the PANI/CC and ERGNO/CC as the anodes reached a stable maximum power density of ~1000 mW m^{-2}, ~820 mW m^{-2} and ~780 mW m^{-2} after 2–3 days operation, which is 2.2, 1.8 and 1.7 times larger than that of the CC anode MFC respectively.

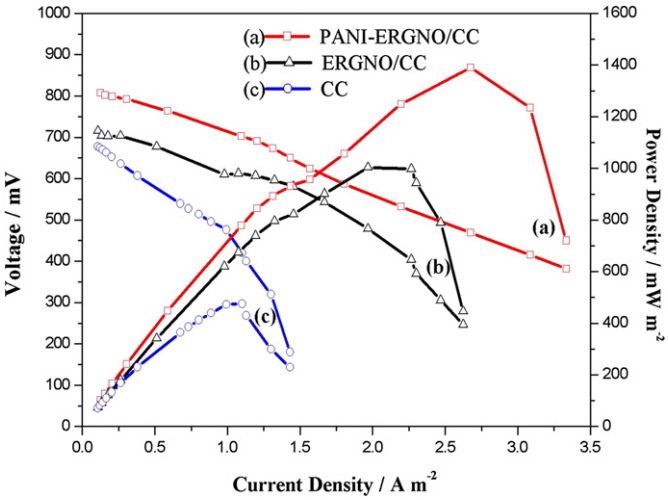

Fig. 7. Polarization curves with PANI–ERGNO/CC (a), ERGNO/CC (b), and CC (c) as the MFC anodes.

Polarization tests were employed to determine the MFCs overall performance with the three modified anodes. As shown in Fig. 7, the open circuit voltage (OCV) of the PANI–ERGNO/CC anode is 0.77 V, larger than that of the ERGNO/CC and the CC anode. Furthermore, the PANI–ERGNO/CC anode MFC achieved a maximum power density of 1390 mW m^{-2} at the current density of 2.67 A m^{-2}, while the maximum power density of the ERGNO/CC MFC was 1003 mW m^{-2} at the current density of 1.97 A m^{-2}. The PANI–ERGNO/CC and ERGNO/CC anodes increased the MFCs power output by 3 and 2.1 times respectively compared with that of the unmodified MFC whose maximum power density is only 468 mW m^{-2} at the current density of 1 A m^{-2}.

4. Conclusions

Graphene synthesis based on electrochemical method is an effective way for electrode modification, the resulting films thickness is uniform, controllable and reproducible, and moreover, toxic chemicals are not involved. The MFCs with the PANI–ERGNO/CC anode yield a maximum power density of 1390 mW m^{-2} which is 3 times larger than the MFC with the CC anode. The great improvement is attributed to the large specific surface area of PANI–ERGNO and its ability to integrate with bacterial biofilm which may greatly increase the bacterial biofilm loading and the charge transfer efficiency. Our experimental results prove that the method proposed in this paper is simple and reliable for fabrication high-performance MFC anodes.

References

[1] B.E. Logan, B. Hamelers, R. Rozendal, U. Schroder, J. Keller, S. Freguia, P. Aelterman, W. Verstraete, K. Rabaey, Environ. Sci. Technol. 40 (2006) 5181–5192.
[2] B.E. Logan, D. Call, S.A. Cheng, H.V.M. Hamelers, T.H.J.A. Sleutels, A.W. Jeremiasse, R.A. Rozendal, Environ. Sci. Technol. 42 (2008) 8630–8640.
[3] J.M. Foley, R.A. Rozendal, C.K. Hertle, P.A. Lant, K. Rabaey, Environ. Sci. Technol. 44 (2010) 3629–3637.
[4] A. Morel, K.C. Zuo, X. Xia, J.C. Wei, X. Luo, P. Liang, X. Huang, Bioresour. Technol. 118 (2012) 43–48.
[5] K.S. Jacobson, D.M. Drew, Z. He, Environ. Sci. Technol. 45 (2011) 4652–4657.
[6] C. Donovan, A. Dewan, H. Peng, D. Heo, H. Beyenal, J. Power Sources 196 (2011) 1171–1177.
[7] P.Y. Zhang, Z.L. Liu, J. Power Sources 195 (2010) 8013–8018.
[8] S.Q. Ci, Z.H. Wen, J.H. Chen, Z. He, Electrochem. Commun. 14 (2012) 71–74.
[9] P. Liang, H.Y. Wang, X. Xia, X. Huang, Y.H. Mo, X.X. Cao, M.Z. Fan, Biosens. Bioelectron. 26 (2011) 3000–3004.
[10] Y. Qiao, C.M. Li, S.J. Bao, Q.L. Bao, J. Power Sources 170 (2007) 79–84.
[11] Z.S. Lv, D.H. Xie, X.J. Yue, C.H. Feng, C.H. Wei, J. Power Sources 210 (2012) 26–31.
[12] M. Batzill, Surf. Sci. Rep. 67 (2012) 83–115.
[13] J. Yan, J.P. Liu, Z.J. Fan, T. Wei, L.J. Zhang, Carbon 50 (2012) 2179–2188.
[14] X.C. Miao, S. Tongay, M.K. Petterson, K. Berke, A.G. Rinzler, B.R. Appleton, A.F. Hebard, Nano Lett. 12 (2012) 2745–2750.
[15] Z.H. Wu, W.C. Ren, L. Xu, F. Li, H.M. Cheng, ACS Nano 5 (2011) 5463–5471.
[16] Y.Z. Zhang, G.Q. Mo, X.W. Li, W.D. Zhang, J.Q. Zhang, J.S. Ye, X.D. Huang, C.Z. Yu, J. Power Sources 196 (2011) 5402–5407.
[17] L. Xiao, J. Damien, J.Y. Luo, H.D. Jang, J.X. Huang, Z. He, J. Power Sources 208 (2012) 187–192.
[18] J. Liu, Y. Qiao, C.X. Guo, S. Lim, H. Song, C.M. Li, Bioresour. Technol. 114 (2012) 275–280.
[19] Y.C. Yong, X.C. Dong, B.C. Park, H. Song, P. Chen, ACS Nano 6 (2012) 2394–2400.
[20] T. Kuilla, S. Bhadra, D.H. Yao, N.H. Kim, S. Bose, J.H. Lee, Prog. Polym. Sci. 35 (2010) 1350–1375.
[21] S.X. Guo, S.F. Zhao, A.M. Bond, J. Zhang, Langmuir 28 (2012) 5275–5285.
[22] W. Hummers, R. Offeman, J. Am. Chem. Soc. 80 (1958) 1339.
[23] H.L. Guo, X.F. Wang, Q.Y. Qian, ACS Nano 3 (2009) 2653–2659.
[24] K. Zhang, L.L. Zhang, X.S. Zhao, Chem. Mater. 22 (2010) 1392–1401.
[25] M. Du, T. Yang, K. Jiao, J. Mater. Chem. 20 (2010) 9253–9260.
[26] Z. He, N. Wagner, S.D. Minteer, L.T. Angenent, Environ. Sci. Technol. 40 (2006) 5212–5217.
[27] M. Du, T. Yang, X. Li, K. Jiao, Talanta 88 (2012) 439–444.
[28] H. Liang, X.J. Miao, J.M. Gong, Electrochem. Commun. 20 (2012) 149–152.
[29] Z.J. Wang, X.Z. Zhou, J. Zhang, F. Boey, H. Zhang, J. Phys. Chem. C 113 (2009) 14071–14075.

[30] J. Yan, T. Wei, B. Shao, Z. Fan, W. Qian, M. Zhang, F. Wei, Carbon 48 (2010) 487.
[31] Z.H. Ni, H.M. Wang, Y. Ma, J. Kasim, Y.H. Wu, Z.X. Shen, ACS Nano 2 (2008) 1033–1039.
[32] A. Gupta, G. Chen, P. Joshi, S. Tadigadapa, P.C. Eklund, Nano Lett. 6 (2006) 2667–2673.
[33] D.W. Wang, F. Li, J.P. Zhao, W.C. Ren, ACS Nano 3 (2009) 1745–1752.
[34] G.Q. Wang, W. Xing, S.P. Zhuo, Electrochim. Acta 66 (2012) 151–157.
[35] Y. Harima, S. Setodoi, I. Imae, K. Komaguchi, Y. Ooyama, J. Ohshita, H. Mizota, J. Yano, Electrochim. Acta 56 (2011) 5363–5368.
[36] J.F. Ping, Y.X. Wang, K. Fan, J. Wu, Y.B. Ying, Biosens. Bioelectron. 28 (2011) 204–209.
[37] Q. Wu, Y.X. Xu, Z.Y. Yao, A.R. Liu, G.Q. Shi, ACS Nano 4 (2010) 1963–1970.
[38] Z. He, F. Mansfeld, Energy Environ. Sci. 2 (2009) 215–219.
[39] F. Zhang, M.D. Merrill, J.C. Tokash, T. Saito, S.A. Cheng, M.A. Hickner, B.E. Logan, J. Power Sources 196 (2011) 1097–1102.